https://doi.org/10.5194/egusphere-2025-768
Preprint. Discussion started: 28 March 2025

Effects of geomagnetic mirror force and pitch angles of precipitating electrons on ionization of the polar upper atmosphere

Tomotaka Tanaka[1], Yasunobu Ogawa[1,2], Yuto Katoh[3], Mizuki Fukizawa[2], Anton Artemyev[4], Vassilis Angelopoulos[4], Xiao-Jia Zhang[5], Yoshimasa Tanaka[1,2,6], Akira Kadokura[2,6]

[1]The Graduate University for Advanced Studies, SOKENDAI
[2]National Institute of Polar Research
[3]Tohoku University
[4]University of California, Los Angeles, UCLA
[5]University of Texas, Dallas, UTD, Dallas
[6]Joint Support-Center for Data Science Research, ROIS, Tokyo

Correspondence to: Tomotaka Tanaka (tanaka.tomotaka@nipr.ac.jp)

Abstract. We studied the effects of the geomagnetic mirror force on electron density enhancements in the polar atmosphere due to energetic electron precipitation. Using pitch angle and energy distribution of electrons observed by the low-altitude Electron Losses and Fields INvestigation (ELFIN) satellites as initial conditions, the electron density in the atmosphere caused by precipitating electrons was calculated by a simulation with two different methods: a traditional method that does not include the effect of the mirror force and a recently developed method that includes the effect. From a simultaneous observation event of the ELFIN satellite and the European Incoherent SCATter scientific radar system (EISCAT) Tromsø radar, it was found that the method with the effect of the mirror force reduces electron density by about 40% at an altitude of 80 km compared to the traditional method. This decrease was pronounced when the pitch angle distribution of high-energy electrons was concentrated in the trapped and boundary regions. The maximum decrease was 50%. It was verified that electron density distribution estimated using the method with the effect of mirror force showed good agreement with an electron density profile derived from the EISCAT radar. The validation of simulation results based on these observation data contributes to the establishment and improvement of atmospheric ionization models using various types of precipitating electrons.

1 Introduction

It has been focused on the impact of energetic electron (> 50 keV) precipitation (EEP) on the ozone. Miyoshi et al. (2020) suggested that precipitating energetic electrons penetrate to low altitudes with the appearance of diffuse auroras. Because the energetic electrons maintain high energy even after passing through the auroral altitude, they have been found to cause electron density enhancement at about 50 km altitude (Oyama et al., 2017). These enhancements may accelerate chemical reactions and the generation of nitrogen or hydrogen oxides to destroy ozone in the mesosphere below 80 km altitude

(Turunen et al., 2016). However, the ionization rates by EEP differ between models up to an order (Nesse et al., 2022). Therefore, it is necessary to evaluate the effects of EEP on the atmosphere accurately by considering simulation improvements.

The mirror force, one of the effects of the magnet field on the charged particles, has recently been considered in numerical simulations of atmospheric ionization by precipitating electrons. As the magnetic field strength at atmospheric altitudes is nearly constant, the change in the pitch angle of precipitating electrons by the effect of the mirror force has been considered negligible (Rees, 1963). Even if some numerical simulations included the pitch angle, it was only used to calculate the altitude change of the electron using the inclination of the magnetic field and pitch angle. Thus, velocity changes due to the mirror force were still ignored (Solomon, 1993, 2001). Recently, a numerical simulation to calculate the altitude profile of atmospheric ionization rate by EEP, including the effect of the mirror force, was developed (Lehtinen et al., 1999), and the results of the simulation were parameterized by the pitch angle and energy of the electron (Xu et al., 2020). Furthermore, using a newly developed simulation, Katoh et al. (2023) showed the concrete difference in ionization rates between with and without the effect of the mirror force. By comparing the simulation results with and without the effect, it was found that when an electron with a large pitch angle had energies above 100 keV, the ionization rate of the former was less than 10% of the latter (Katoh et al., 2023). However, actual data has not yet confirmed this.

Although some satellites have observed electrons' energy and pitch angle distribution, it has been challenging to use them in the simulation as input. Arase satellite, for example, is too far away to observe the pitch angle distribution of electrons reaching the earth's atmosphere in detail, while the energy range of electrons observed by the Reimei satellite was too low to make differences between with and without the effect of the mirror force, as shown in Katoh et al. (2023). However, the satellite, a polar-orbiting and low-altitude satellite, observed both pitch angle and energy distribution of energetic electrons. Therefore, it has been possible to evaluate the actual atmospheric effects by combining the satellite with the simulations developed by Katoh et al. (2023).

This study aims to evaluate the effect of the mirror force on atmospheric electron density using the satellite and the simulations and to validate the results using the radar. Even though it is challenging to evaluate the ionization rate, calculating the electron density from the ionization rate enabled us to compare it with observational data. Using the pitch angle and energy distributions of electrons observed by the ELFIN (Electron Losses and Fields INvestigation CubeSats) satellite, we calculated the electron density enhancement due to the precipitating electrons with and without the effect separately to compare them with the actual data observed by the EISCAT (European Incoherent Scatter) Tromsø radar.

https://doi.org/10.5194/egusphere-2025-768
Preprint. Discussion started: 28 March 2025

2 Methods and Instruments

2.1 ELFIN satellite

We used data from the ELFIN satellite. The satellite was launched in September 2018 and completed observations in September 2022. It is on a low-altitude (~450 km altitude) polar orbit (~93°inclination), and the orbital period is about 90 min. It consists of two CubeSats (ELFIN-A/B), flying in nearly identical orbits with a time difference of less than 20 min (Angelopoulos et al., 2020). Each satellite had an energy particle detector for electrons (EPDE), which measured 50 – 7000 keV electrons with $\Delta E/E < 40\%$ energy resolution and 22.5° pitch angle resolution. Since the electron flux above 2500 keV is negligible compared to electrons with energies below that, we used the electron flux data between 50 and 2500 keV in this study. The spin axis is kept perpendicular to the orbital plane, and the whole pitch angle is observed twice every spin period (~2.85 s) (Zhang et al., 2022). The loss cone angle was defined as the angle at which the pitch angle would be 90 degrees at 100 km altitude if an electron moves with the Lorentz force due to the geomagnetic field.

2.2 EISCAT UHF/VHF Tromsø radar

We also used the EISCAT radar, which has been operated in Northern Scandinavia since 1981 and in Svalbard since 1996. One of the radars is located at Tromsø (69.6ºN, 19.2ºE, and magnetic latitude of 66º), which observes the altitude profile of electron density and other ionospheric parameters (Folkestad, K., 1983).

2.3 Simulation

The simulation used in this study is a Monte Carlo simulation developed by Katoh et al. (2023). It has atmospheric data of oxygen atoms, oxygen molecules, and nitrogen molecules using the pymsis model (Lucas, 2022; Emmert et al., 2020; Emmert et al., 2022; Picone et al., 2002; Celestrak; Matzka et al., 2021). It enables us to calculate the altitude profile of the ionization rate above Tromsø (L=6.45) using the data of an electron as initial conditions such as altitude, pitch angle, and energy. The effect of Lorentz force can be included or excluded manually when calculating particle transport. When considering the force, the magnetic field at a distance of Larmor radius from the magnetic field line leading to Tromsø was given to satisfy $\nabla \cdot \boldsymbol{B}=0$ and used in the calculations.

2.4 Combination of the ELFIN satellite data and simulation

First, we searched for events in which the ELFIN satellite approached the EISCAT Tromsø radar, which was defined as the situation in which the geomagnetic coordinate of the satellite was in the region 69.6ºN ± 2º, 19.2ºE ± 5º. Second, we selected events that showed some electron density peak under 100 km altitudes or had a density of more than 10^{10} m^{-3} at 85 km altitude in the EISCAT data, which should be caused by the EEP. Next, we used the data in each pitch angle/energy bin observed by the ELFIN satellite as the initial condition of simulations to calculate the altitude profile of collision rate

https://doi.org/10.5194/egusphere-2025-768
Preprint. Discussion started: 28 March 2025

R [m^{-1}], that is, the number of ionization events a precipitating electron made in the atmosphere during its 1 m movement at the altitude. For some specific bins containing the loss cone angle, the collision rate was calculated more precisely. In other words, we divided the pitch angle range of the bin into ten parts to simulate separately, and we averaged these ten results. This is because simulation results near the loss cone angle vary significantly depending on the initial pitch angle. The results of each simulation were integrated depending on the observed range of energy and pitch angle. The differential number flux f [$\mathrm{s}^{-1}\mathrm{m}^{-2}\mathrm{str}^{-1}\mathrm{MeV}^{-1}$] observed by the satellite was integrated according to the observed range of energy and pitch angle to obtain the total number flux F [$\mathrm{s}^{-1}\mathrm{m}^{-2}$]. It was multiplied by R to obtain the ionization rate Q [$\mathrm{m}^{-3}\mathrm{s}^{-1}$]. The electron density is estimated from the rate Q using the following method. The time variation of the electron density due to production and recombination is

$$\frac{\mathrm{d}N_e}{\mathrm{d}t} = Q - \alpha {N_e}^2 \tag{1}$$

where α [$\mathrm{m}^3\mathrm{s}^{-1}$] is an effective recombination rate of Gledhill (1986), and N_e [m^{-3}] is the electron density. As the time variation of electron density can be assumed to be smaller than the time resolution of the observation, we got the electron density as $N_e = \sqrt{\frac{Q}{\alpha}}$. Then, the altitude profile of electron density was calculated both with and without consideration of the effect of the mirror force. The ratio of the density with the effect to that without the effect at 80 km altitude is used as a measure of the mirror force effect and, hereinafter, is called the "density ratio." We showed the density ratios at an altitude of 80 km as representative values in this paper. Finally, a comparison was made between simulations and observations of the altitude profile of electron density during the 15 seconds when the footprint of the satellite and the radar are closest.

3 Results

3.1 Event on December 16, 2021

There were five events that the ELFIN satellite and the EISCAT Tromsø radar observed simultaneously, and the electron density increased under 100 km altitude. Especially in the event on December 16, 2021, at about 07:14 UT, the satellite footprint was the closest to the radar, and they were thought to be under simultaneous observation of an electron density enhancement in the atmosphere caused by EEP. In this event, the *AE* index was up to 300 nT, and geomagnetic pulsations were found. The solar wind was quiet, with Bz at -2 nT and SYM-H at -16 nT. Figure 1 shows the footprints of the ELFIN-A for about 5 min from around 07:12 UT and the location of EISCAT Tromsø radar. The satellite traveled southward and was closest to the radar around 7:14:30 UT. The red dots show the satellite position during the 15 seconds we used the observation data in this study.

Figure 2a shows that the EISCAT Tromsø radar data observed electron density enhancement that the value was more than 2×10^{10} m^{-3} for 10 min and that it had double peaks when the satellite was the closest to the radar, one was at 104.8 km altitude, and the other was at 94.7 km altitude in the electron density profile. It is assumed that an EEP observed by the

https://doi.org/10.5194/egusphere-2025-768
Preprint. Discussion started: 28 March 2025

satellite made the second peak. Figure 2b shows the isotropic pitch angle distribution of electrons in the north of the radar, while most of the electrons had larger pitch angles than the loss cone angle at the southern range. It was also observed in Fig. 2c that most of the energetic electrons above 500 keV were with large pitch angles, regardless of location. Figures 2d and 2e show that at the closest approach time, electrons with energy above 1000 keV were observed and that trapped electrons were major above 100 keV. Figure 2f shows the fraction of energy flux of precipitating, boundary, and trapped electrons separately among electrons with energy between 50 and 2500 keV. Note that the "boundary electrons" are defined as electrons observed in bins of equipment whose observation range includes the loss cone angle. Figure 2g is the density ratio at 80 km altitude, and Fig. 2h is the location of the ELFIN satellite. The time range in Figs. 2f and 2g are restricted between 07:13 and 07:16 because the number of electrons observed by the satellite at other times was not enough to be analyzed meaningfully. These three figures were compared in order to investigate trends in the density ratio. The density ratio decreased as the satellite went south; that is, *the* L-value and the invariant latitude got smaller, and simultaneously, the ratio of trapped and boundary electrons became larger. For example, the density ratio was 0.8 at maximum when the trapped electrons occupied about half of the energy flux at the location with the L-value of 10 and the invariant latitude of 72^{o}. On

https://doi.org/10.5194/egusphere-2025-768
Preprint. Discussion started: 28 March 2025

the other hand, the value was 0.5 at minimum when the L-value was five, and the invariant latitude was 63°. The trapped and boundary electrons were responsible for more than 75% of the total energy flux. The density ratio was especially 0.6 at the point where the footprint of the ELFIN satellite was the closest to the radar. In other words, we can say that the density ratio became smaller as the electrons with large pitch angles were more dominant in the distributions.

Figure 1: The footprint of the ELFIN satellite (black and red dots) and the location of the EISCAT Tromsø radar (yellow star). The red ones show the satellite footprint for 15 s when both were the closest during the event.

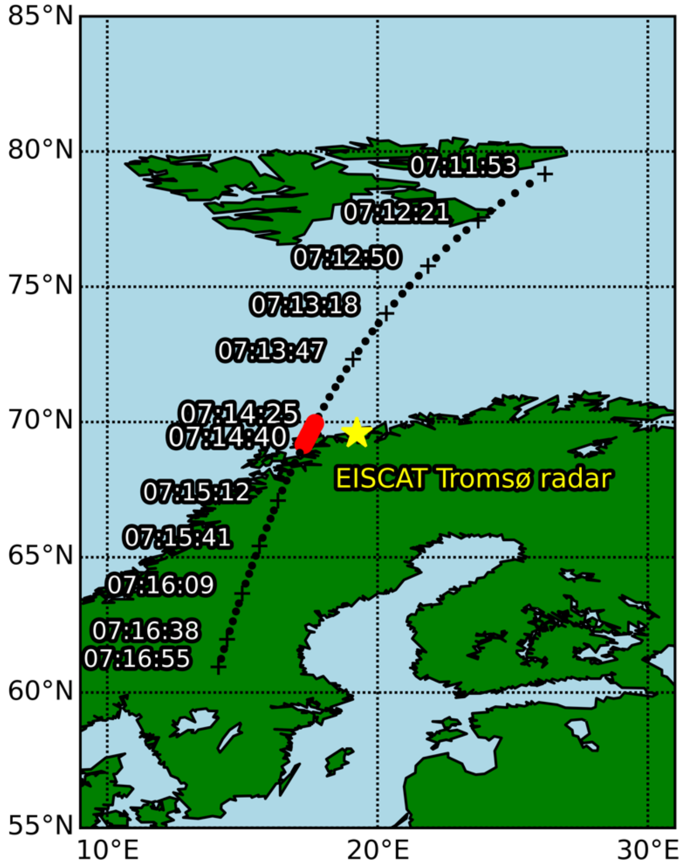

https://doi.org/10.5194/egusphere-2025-768
Preprint. Discussion started: 28 March 2025

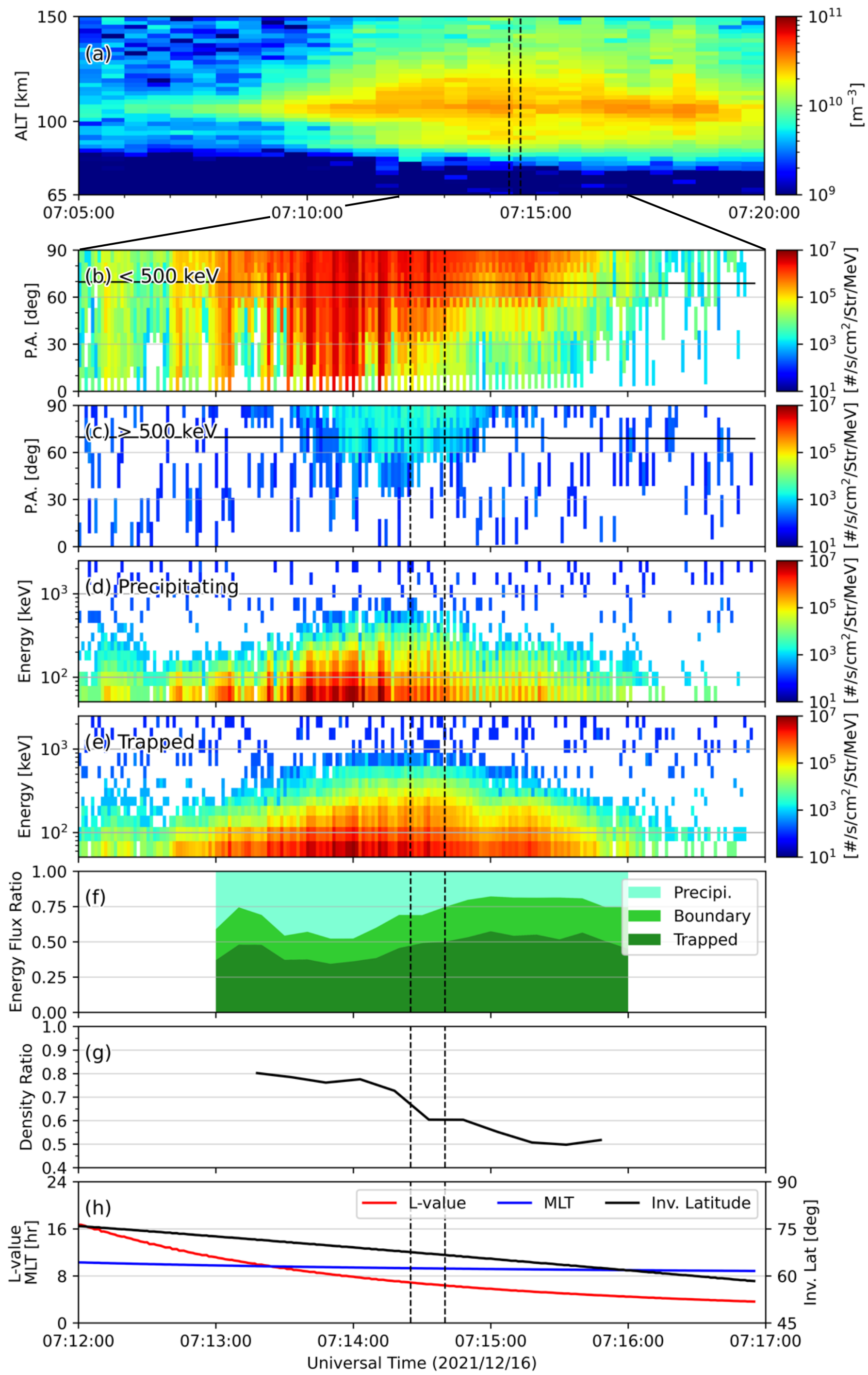

https://doi.org/10.5194/egusphere-2025-768
Preprint. Discussion started: 28 March 2025

Figure 2: Simultaneous observation data of the EISCAT Tromsø radar (a) and the ELFIN satellite (b-f), and the simulation result (g). (a) Altitude profile of electron density observed by the EISCAT. (b) Average pitch angle distributions of the electron number flux below 500 keV were observed by the satellite. (c) Same as (b) but for that above 500 keV. (d) Average energy distributions of the electrons with the pitch angles less than the loss cone angle. (e) Same as (d) but for those more than the loss cone angle. (f) Fraction of the energy flux for precipitating, boundary, and trapped electrons. (g) The density ratio at 80 km altitude from the simulations with/without mirror force effect. (h) Information on the geomagnetic location of the satellite: L-value, magnetic local time, and invariant latitude. Two vertical dashed lines show the 15 s time span of the closest approach of the satellite to the EISCAT, corresponding to the red dots in Fig. 1.

3.2 Data of the ELFIN satellite

Figure 3 shows the pitch angle and energy distribution of the electron number flux observed by the ELFIN satellite. The time range of Fig. 3(b) includes the time of closest approach of the satellite to the EISCAT Tromsø radar. As mentioned in the introduction, the effect of mirror force is essential mainly for electrons with large pitch angles and with energy more than 100 keV. According to Fig. 3(b), most electrons with energy less than 1000 keV had large pitch angles, though the pitch angle distribution of electrons with higher energy than 1000 keV did not show any apparent tendencies. Specifically, the number flux of electrons with 63 keV electrons, for example, was about $10^6\ \mathrm{s^{-1}cm^{-2}str^{-1}MeV^{-1}}$ with a pitch angle larger than 70° while that was less than $10^5\ \mathrm{s^{-1}cm^{-2}str^{-1}MeV^{-1}}$ with a pitch angle less than 30°. The analysis for the entire observed energy range revealed that the electrons with pitch angles almost equal to or greater than the loss cone angle account for about 72% of the total energy flux.

The distributions in Figs. 3(a) and 3(c) are the same as in Fig. 3(b) except for observation time, which has time ranges of 10 s before and after the time of Fig. 3(b). Even though the satellite did not pass through just above the radar, it can be estimated that electrons should have a similar distribution above the radar because the distribution was almost the same in a wide area, as shown in Fig. 3.

https://doi.org/10.5194/egusphere-2025-768
Preprint. Discussion started: 28 March 2025

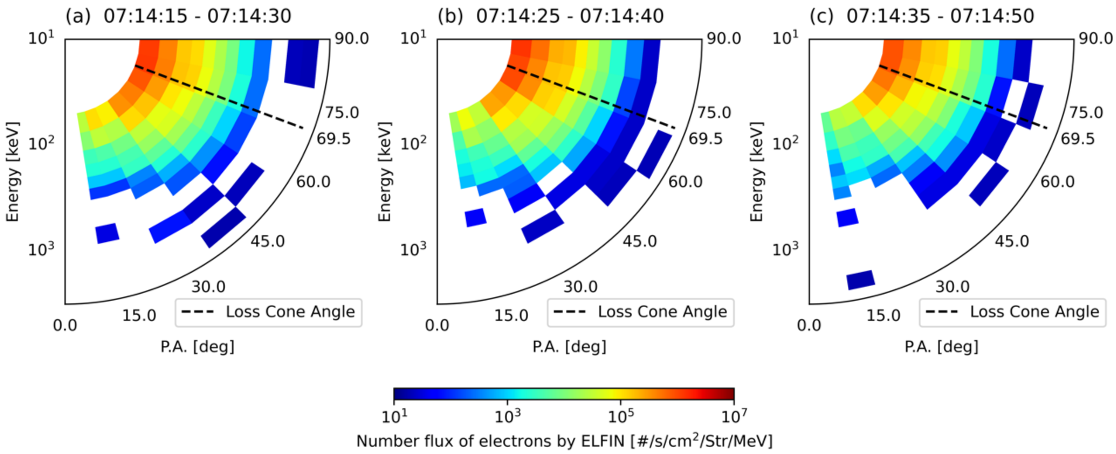

Figure 3: Pitch angle and energy distribution of the electron number flux observed by the ELFIN satellite, averaged during 15 s before (a), at the time (b), and after (c) the closest access of the satellite to the EISCAT Tromsø radar. Dashed lines indicate the loss cone angle.

3.3 Simulation results and comparison with EISCAT observation data

Figure 4 shows three types of altitude profiles of the electron density. The black line is the EISCAT Tromsø radar data, while the red and blue lines are simulated electron density using the electron distribution shown in Fig. 3(b) as an initial condition with and without the mirror force effect, respectively. Each peak value at 87 km altitude of red and blue lines in Fig. 4 is made by 63 keV electrons, which is the minimum value of observed energy. Because electrons with energy less than 63 keV, out of observation, must have contributed to the atmospheric electron density above 87 km altitude, we compared the simulation results to the radar data at altitudes below 85 km (see Zou et al., 2024). The density ratio between the simulations with and without the mirror force effect is 0.6 at 80 km altitude, and the value does not change significantly in the altitude range below 85 km. The density ratio between the "with simulation" ("without simulation") and the EISCAT observation at 80 km is 1.7 (2.9), respectively. Hence, it can be said that the mirror force effect is essential for studying the ionization process by the EEP at altitudes below 85 km.

https://doi.org/10.5194/egusphere-2025-768
Preprint. Discussion started: 28 March 2025

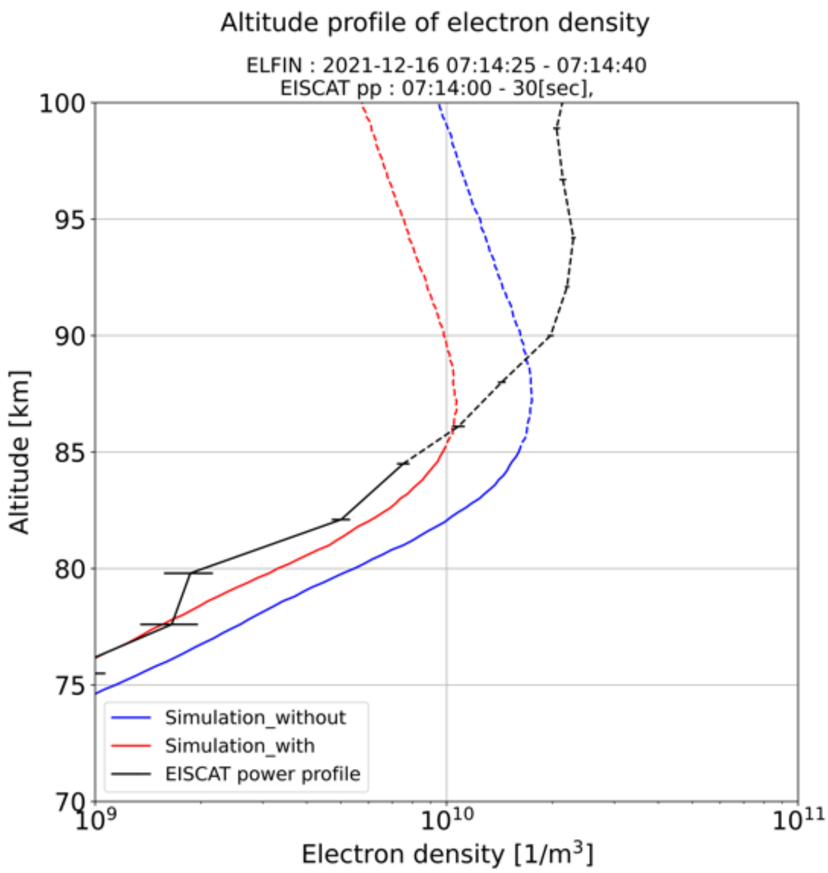

Figure 4: Altitude profile of electron density. Simulation results, with/without the mirror force effect, are shown by the red/blue lines, respectively. The black line shows the EISCAT Tromsø radar observation. Note that it is inappropriate to compare simulation results with the observed data above 85 km altitude because there must be an electron density enhancement due to lower energy electrons than observed by the ELFIN satellite.

3.4 The results of the other events and their characteristics

We investigated five events, including the one described in Section 3. Table 1 shows the date, MLT, the density ratio at 80 km altitude, the energy flux percentage of trapped electrons, including boundary electrons (Tra. E-flux), and information on the aurora and *AE* index. We calculated these values using data of the time when the ELFIN satellite was closest approach to the EISCAT Tromsø radar at the magnetic latitude of 66°.

The density ratios were between 0.56 and 0.87. When the value was the smallest, that was 0.56, trapped or boundary electrons accounted for 80% of the total energy flux. When the value was the maximum of 0.87, on the other hand, trapped or boundary electrons had 35% energy flux, which is less than half of the former; thus, the pitch angle distribution was close

https://doi.org/10.5194/egusphere-2025-768
Preprint. Discussion started: 28 March 2025

to isotropic. In addition, it was ~10 min before the maxima of the horizontal geomagnetic component in Tromsø, and the peak of the AL decreased. Therefore, it was confirmed that the magnetic condition changed the pitch angle distribution, i.e., the density ratio. It was found that, as mentioned in Katoh et al. (2023), electrons with large pitch angles make a difference due to the mirror force, reducing the electron density resulting from actual distribution by approximately half compared to the traditional method, which ignored the mirror force.

Focusing on whole events, the MLT distribution shows that differences due to the mirror force appear in the order of before midnight, at night, and in the morning. On the other hand, the *AE* index does not look like the key to the difference.

Table 1. Summary of conjunction events between the ELFIN satellite and EISCAT Tromsø radar

Date yy/mm/dd	UT MLT [hr]	Density ratio	Tra. E-flux	Camera data *AE* index
20/12/09	21:31 23.2	0.87	35%	Cloudy *AE* ~ 200 nT
21/01/07	19:52 21.5	0.65	93%	Diffuse aurora *AE* ~ 100 nT
21/10/05	20:20 22.4	0.64	61%	Cloudy *AE* ~ 100 nT
21/11/27	07:36 9.9	0.56	80%	No observation *AE* ~ 50 nT
21/12/16	07:14 9.7	0.61	72%	No observation *AE* ~ 350 nT

4 Discussion

Table 1 compares the density ratios at 80 km altitude with the MLT and the percentages of energy fluxes to identify the conditions under which differences due to the mirror force appeared. A value "pre/tra ratio" is the ratio of energy flux of precipitating electrons to trapped electrons. The MLT distribution of the pre/tra ratio was statistically analyzed with *AE* index classification (Qin et al., 2023; Tsai et al., 2024). Compared to the results of these studies, the results of our study were almost consistent with a larger proportion of pre/tra ratio in the order of before midnight, at night, and in the morning, as mentioned in the last section. In the 7 Jan. event, its value is out of trend, but that is because the percentage of boundary electrons energy flux was 50% and could not be meaningfully calculated. Although the images could not be analyzed in this study because they were unavailable, they seem related to the type of aurora. For instance, precipitating electrons from the radiation belt due to the wave-particle interaction are thought to have a relatively small pre/tra ratio because they originally

https://doi.org/10.5194/egusphere-2025-768
Preprint. Discussion started: 28 March 2025

had a large pitch angle to maintain the region. In fact, the density ratio was relatively small at 0.65 for the 7 Jan. event when the diffuse aurora was observed. In addition, the point that larger values of the *AE* index were associated with larger values of the pre/tra ratio is partly consistent with ours. In other words, the 16 Dec. event with 350 nT *AE* index in Fig 2f showed an increase in the pre/tra ratio along with the *L* value, which is consistent with the previous study.

To compare the altitude profile of electron density, the simulation results and observational data were in good agreement for the December 16 event (see Fig. 4), but not necessarily for the other events. One reason is mainly due to the spatial distance between the ELFIN satellite and the EISCAT Tromsø radar, but more accurate simulations are needed to compare its results to observational data, such as the introduction of secondary electrons. In detail, Fig. 4 also showed a minor disagreement between observation and simulation results. The event is characterized by intense bursty precipitations, most likely due to electrons scattered by whistler-mode waves (e.g., Zhang et al., 2023). In that case, the electron flux is expected to vary on a time-scales of seconds, but the satellite could not capture it within a limited latitude range conjugated to the radar.

The ionization profile during EEP is affected not only by pitch angle distribution but also by energy distribution. Katoh et al. (2023) found that the difference due to the consideration of the mirror force becomes more evident for electrons with higher energy. Additionally, the pre/tra energy flux ratio of electrons always decreases with energy when EEP occurs due to the whistler-mode waves (e.g., Tsai et al., 2023). Both results support the idea that higher energy electrons are more likely to be affected by the mirror force, which reduces the electron density in the atmosphere. On the other hand, it is known that the ratio sometimes remains constant for the 50-1000 keV range during intense precipitations by high-intense waves (Zhang et al., 2022) and that the ratio increases if precipitation is driven by EMIC waves (Capannolo et al., 2023). These studies suggest that the significance of the effect of the mirror force depends on the wave strength or types, but we only found whistler-mode wave events in our conjugated observation. Therefore, it is necessary to statistically investigate the force's contribution to the electron density in the atmosphere with a focus on the type of wave.

In this study, we also examined the latitudinal distribution of the density ratio for only one event (see Fig. 2(g)). We found that the difference due to the mirror force depends on the latitude and that the ratio is more likely small as the latitude is low, even while electrons seemed to be precipitating from the radiation belt. This is because the distribution of electrons depends on the latitude. Specifically, this is because the percentage of trapped electrons was more significant at lower latitudes. It is also statistically consistent with Qin's finding that the smaller the L value, the smaller the pre/tra ratio. However, the effects of the mirror force, i.e., the variations in density ratios due to distribution changes in both the energy and pitch angle, are not yet fully understood, so more ELFIN satellite observation events should be used to examine the latitudinal distribution of the ratio.

Finally, this study focused on the magnetic mirror force and included its effects in the simulation to see how it changes the electron density enhancement in the atmosphere. It was mentioned in Katoh et al. (2023) that some electrons move back toward away from the atmosphere, i.e., go up again. However, even though the ELFIN satellite observed the flux of upgoing electrons, a comparison between the observational data and the simulation results has yet to be made. In the future, it can be verified whether the upgoing electrons observed would be consistent with the simulation results by improving the simulation code so that the energy and pitch angle distributions of the reflected electrons can be calculated.

5 Conclusion

This study aims to evaluate the effect of the mirror force on precipitating electrons and, consequently, atmospheric electron density by focusing on the pitch angle of the electrons. We used ELFIN satellite data and a simulation developed by Katoh et al. (2023). We found that the electron density by EEP can be about 40% smaller when the effect of the mirror force is considered than when the result ignored the effect as in previous studies (e.g., Murase et al., 2023). The result was validated using the EISCAT Tromsø radar; the simulated electron density, including the effect, is closer to the actual value than ignoring it. Furthermore, although this is not a conjunction event between the ELFIN satellite and the radar, some pitch angle distribution made the ratio 50% at maximum. In other words, these results suggest the importance of considering the pitch angle distribution of electrons and the effect of EEP on the simulation of electron density enhancement in the atmosphere, or the result would get half of the error value. In addition, satellite electron observations at low altitudes should observe pitch angle distributions with high resolution that can at least distinguish trapped or precipitating particles.

Acknowledgments

This research was supported by the Grants-in-Aid for Scientific Research (20K04052, 20KK0313, and 23H05429) by the Ministry of Education, Science, Sports and Culture, Japan.

References

Angelopoulos, V., Tsai, E., Bingley, L., Shaffer, C., Turner, D. L., Runov, A., Li, W., Liu, J., Artemyev, A. V., Zhang, X.-J., Strangeway, R. J., Wirz, R. E., Shprits, Y. Y., Sergeev, V. A., Caron, R. P., Chung, M., Cruce, P., Greer, W., Grimes, E., Hector, K., Lawson, M. J., Leneman, D., Masongsong, E. V., Russell, C. L., Wilkins, C., Hinkley, D., Blake, J. B., Adair, N., Allen, M., Anderson, M., Arreola-Zamora, M., Artinger, J., Asher, J., Branchevsky, D., Capitelli, M. R., Castro, R., Chao, G., Chung, N., Cliffe, M., Colton, K., Costello, C., Depe, D., Domae, B. W., Eldin, S., Fitzgibbon, L., Flemming, A., Fox, I., Frederick, D. M., Gilbert, A., Gildemeister, A., Gonzalez, A., Hesford, B., Jha, S., Kang, N., King, J., Krieger, R., Lian, K., Mao, J., McKinney, E., Miller, J. P., Norris, A., Nuesca, M., Palla, A., Park, E. S. Y., Pedersen, C. E., Qu, Z., Rozario, R., Rye, E., Seaton, R., Subramanian, A., Sundin, S. R., Tan, A., Turner, W., Villegas,

https://doi.org/10.5194/egusphere-2025-768
Preprint. Discussion started: 28 March 2025

A. J., Wasden, M., Wing, G., Wong, C., Xie, E., Yamamoto, S., Yap, R., Zarifian, A., and Zhang, G. Y.: The ELFIN Mission, Space Sci Rev, 216, 103, https://doi.org/10.1007/s11214-020-00721-7, 2020.

Capannolo, L., Li, W., Ma, Q., Qin, M., Shen, X.-C., Angelopoulos, V., Artemyev, A., Zhang, X.-J., and Hanzelka, M.: Electron Precipitation Observed by ELFIN Using Proton Precipitation as a Proxy for Electromagnetic Ion Cyclotron (EMIC) Waves, Geophysical Research Letters, 50, e2023GL103519, https://doi.org/10.1029/2023GL103519, 2023.

CelesTrak. https://celestrak.org/SpaceData/

Emmert, J. T., Drob, D. P., Picone, J. M., Siskind, D. E., Jones Jr., M., Mlynczak, M. G., Bernath, P. F., Chu, X., Doornbos, E., Funke, B., Goncharenko, L. P., Hervig, M. E., Schwartz, M. J., Sheese, P. E., Vargas, F., Williams, B. P., and Yuan, T.: NRLMSIS 2.0: A Whole-Atmosphere Empirical Model of Temperature and Neutral Species Densities, Earth and Space Science, 8, e2020EA001321, https://doi.org/10.1029/2020EA001321, 2021.

Emmert, J. T., Jones Jr, M., Siskind, D. E., Drob, D. P., Picone, J. M., Stevens, M. H., Bailey, S. M., Bender, S., Bernath, P. F., Funke, B., Hervig, M. E., and Pérot, K.: NRLMSIS 2.1: An Empirical Model of Nitric Oxide Incorporated Into MSIS, Journal of Geophysical Research: Space Physics, 127, e2022JA030896, https://doi.org/10.1029/2022JA030896, 2022.

Folkestad, K., Hagfors, T., and Westerlund, S.: EISCAT: An updated description of technical characteristics and operational capabilities, Radio Science, 18, 867–879, https://doi.org/10.1029/RS018i006p00867, 1983.

Gledhill, J. A.: The effective recombination coefficient of electrons in the ionosphere between 50 and 150 km, Radio Science, 21, 399–408, https://doi.org/10.1029/RS021i003p00399, 1986.

Katoh, Y., Rosendahl, P. S., Ogawa, Y., Hiraki, Y., and Tadokoro, H.: Effect of the mirror force on the collision rate due to energetic electron precipitation: Monte Carlo simulations, Earth Planets Space, 75, 117, https://doi.org/10.1186/s40623-023-01871-y, 2023.

Lehtinen, N. G., Bell, T. F., and Inan, U. S.: Monte Carlo simulation of runaway MeV electron breakdown with application to red sprites and terrestrial gamma ray flashes, Journal of Geophysical Research: Space Physics, 104, 24699–24712, https://doi.org/10.1029/1999JA900335, 1999.

Lucas, G. (2022). pymsis [Computer software]. doi:10.5281/zenodo.5348502

Matzka, J., Stolle, C., Yamazaki, Y., Bronkalla, O., and Morschhauser, A.: The Geomagnetic Kp Index and Derived Indices of Geomagnetic Activity, Space Weather, 19, e2020SW002641, https://doi.org/10.1029/2020SW002641, 2021.

Miyoshi, Y., Saito, S., Kurita, S., Asamura, K., Hosokawa, K., Sakanoi, T., Mitani, T., Ogawa, Y., Oyama, S., Tsuchiya, F., Jones, S. L., Jaynes, A. N., and Blake, J. B.: Relativistic Electron Microbursts as High-Energy Tail of Pulsating Aurora Electrons, Geophysical Research Letters, 47, e2020GL090360, https://doi.org/10.1029/2020GL090360, 2020.

Murase, K., Kataoka, R., Nishiyama, T., Sato, K., Tsutsumi, M., Tanaka, Y., Ogawa, Y., and Sato, T.: Atmospheric Ionizations by Solar X-Rays, Solar Protons, and Radiation Belt Electrons in September 2017 Space Weather Event, Space Weather, 21, e2023SW003651, https://doi.org/10.1029/2023SW003651, 2023.

Nesse Tyssøy, H., Sinnhuber, M., Asikainen, T., Bender, S., Clilverd, M. A., Funke, B., van de Kamp, M., Pettit, J. M., Randall, C. E., Reddmann, T., Rodger, C. J., Rozanov, E., Smith-Johnsen, C., Sukhodolov, T., Verronen, P. T., Wissing, J. M., and Yakovchuk, O.: HEPPA III Intercomparison Experiment on Electron Precipitation Impacts: 1. Estimated Ionization Rates During a Geomagnetic Active Period in April 2010, Journal of Geophysical Research: Space Physics, 127, e2021JA029128, https://doi.org/10.1029/2021JA029128, 2022.

Oyama, S., Kero, A., Rodger, C. J., Clilverd, M. A., Miyoshi, Y., Partamies, N., Turunen, E., Raita, T., Verronen, P. T., and Saito, S.: Energetic electron precipitation and auroral morphology at the substorm recovery phase, Journal of Geophysical Research: Space Physics, 122, 6508–6527, https://doi.org/10.1002/2016JA023484, 2017.

Picone, J. M., Hedin, A. E., Drob, D. P., and Aikin, A. C.: NRLMSISE-00 empirical model of the atmosphere: Statistical comparisons and scientific issues, Journal of Geophysical Research: Space Physics, 107, SIA 15-1-SIA 15-16, https://doi.org/10.1029/2002JA009430, 2002.

Qin, M., Li, W., Shen, X.-C., Angelopoulos, V., Selesnick, R., Capannolo, L., Ma, Q., Artemyev, A., and Zhang, X.-J.: Global Survey of Energetic Electron Precipitation at Low Earth Orbit Observed by ELFIN, Geophysical Research Letters, 51, e2023GL105134, https://doi.org/10.1029/2023GL105134, 2024.

Rees, M. H.: Auroral ionization and excitation by incident energetic electrons, Planetary and Space Science, 11, 1209–1218, https://doi.org/10.1016/0032-0633(63)90252-6, 1963.

Solomon, S. C.: auroral electron transport using the Monte Carlo Method, Geophysical Research Letters, 20, 185–188, https://doi.org/10.1029/93GL00081, 1993.

Solomon, S. C.: Auroral particle transport using Monte Carlo and hybrid methods, Journal of Geophysical Research: Space Physics, 106, 107–116, https://doi.org/10.1029/2000JA002011, 2001.

Tsai, E., Artemyev, A., Anglelopoulos, V., and Zhang, X.-J.: Investing Whistler-Mode Intensity Along Field Lines Using Electron Precipitation Measurements, Journal of Geophysical Research: Space Physics, 128, e2023JA031578, https://doi.org/10.1029/2023JA031578, 2023.

Tsai, E., Artemyev, A., Ma, Q., Mourenas, D., Agapitov, O., Zhang, X.-J., and Angelopoulos, V.: Key Factors Determining Nightside Energetic Electron Losses Driven by Whistler-Mode Waves, Journal of Geophysical Research: Space Physics, 129, e2023JA032351, https://doi.org/10.1029/2023JA032351, 2024.

Turunen, E., Kero, A., Verronen, P. T., Miyoshi, Y., Oyama, S.-I., and Saito, S.: Mesospheric ozone destruction by high-energy electron precipitation associated with pulsating aurora, Journal of Geophysical Research: Atmospheres, 121, 11,852-11,861, https://doi.org/10.1002/2016JD025015, 2016.

Xu, W., Marshall, R. A., Tyssøy, H. N., and Fang, X.: A Generalized Method for Calculating Atmospheric Ionization by Energetic Electron Precipitation, Journal of Geophysical Research: Space Physics, 125, e2020JA028482, https://doi.org/10.1029/2020JA028482, 2020.

https://doi.org/10.5194/egusphere-2025-768
Preprint. Discussion started: 28 March 2025

Zhang, X.-J., Angelopoulos, V., Mourenas, D., Artemyev, A., Tsai, E., and Wilkins, C.: Characteristics of Electron Microburst Precipitation Based on High-Resolution ELFIN Measurements, Journal of Geophysical Research: Space Physics, 127, e2022JA030509, https://doi.org/10.1029/2022JA030509, 2022.

Zhang, X.-J., Angelopoulos, V., Artemyev, A., Mourenas, D., Agapitov, O., Tsai, E., Wilkins, C.: Temporal Scales of Electron Precipitation Driven by Whistler-Mode Waves, Journal of Geophysical Research: Space Physics, 128, e2022JA031087, https://doi.org/10.129/2022JA031087, 2023.

Zou, Y., Zhang X.-J., Artemyev, A., Shen, Y., and Angelopoulos, V.: The Key Role of Magnetic Curvature Scattering in Energetic Electron Precipitation During Substorm, Journal of Geophysical Research Letters, 51, e2024GL109227, https://doi.org/10.1029/2024GL109227, 2024.